Q. J. R. Meteorol. Soc. (2002), **128**, pp. 477–499

Cloud-top striations above ana-cold frontal circulations

By K. A. BROWNING* and C.-G. WANG
University of Reading, UK

(Received 21 May 2001; revised 26 September 2001)

SUMMARY

Satellite images occasionally show regular arrays of cloud-top striations within mesoscale cloud features associated with vigorous ana-cold frontal circulations. Observational case-studies with a variety of types of radar are presented to show that the striations are due to bands of upright upper-level convective cells. These convective cells form at the top of the rearward-sloping-ascent part of a transverse frontal circulation which, in one of the cases studied, had a multi-layered structure fed in turn by upright line convection lifting air from the boundary layer. This coexistence and interdependence of upright and slantwise forms of convection may not in itself be uncommon; what is less usual in these results is the way in which the upper-level convection is manifested as bands, or striations, orientated roughly parallel to the wind shear at cloud-top level but almost perpendicular to the strong thermal-wind shear in the underlying frontal zone—a behaviour that may be specific to vigorous ana-cold frontal systems. The striations have a large wavelength (30 to 55 km) but we are unaware of any simple dynamical mechanism that can account for the convection being organized on this scale. The striations are regarded as an important indicator of accompanying adverse weather. Earlier studies have suggested that such striations are associated with rapid cyclogenesis and surface gusts. One of the cases presented here falls into this category; the other, more detailed, case-study is notable for the rainfall associated with the vigorous frontal circulations.

KEYWORDS: Convection Doppler radar Fronts Mesoscale Satellite imagery Wind profiler radar

1. INTRODUCTION

This paper addresses a mesoscale cloud phenomenon that occurs sometimes in association with vigorous ana-cold frontal circulations. The primary dynamical characteristic of an ana-cold front is a thermally direct circulation in which rearward-sloping ascent (RSA) of warm air is undercut by forward-sloping descent (FSD) of cold air. In cold-season ana-cold fronts, initial ascent of the warm air is often short-circuited by a line of shallow upright convection (line convection) which lifts air out of the boundary layer into the region of RSA (see review by Browning 1990). Strong line convection, when it occurs, tends to be situated at the position of the surface cold front (SCF). In the UK it is often characterized by convective instability that is rather weak (Browning and Pardoe 1973). There is very strong cyclonic shear across the SCF, and the locally vigorous ascent within the line convection is related to frictional convergence of air originating close to the ground. The line convection produces a narrow cold-frontal rainband (NCFR) about 3 km wide, and the RSA that it feeds gives rise to a wide cold-frontal rainband (WCFR) up to 100 km across (Hobbs 1978). The line convection is usually broken into line elements giving rise to narrow precipitation cores along the SCF with length typically between 5 and 30 km (see Wakimoto and Bosart (2000) for literature survey). Also the slantwise circulation corresponding to the RSA and FSD is sometimes broken up into multiple circulations, stacked vertically with a relatively small vertical scale of about 2 km. Browning *et al.* (2001a) attribute these stacked circulations to the release of conditional symmetric instability (CSI, Bennetts and Hoskins 1979) and to the process of ΔM adjustment whereby air lofted by the line convection has a negative anomaly of absolute geostrophic momentum, M, at the top of the line convection and ascends slantwise as RSA in order to restore geostrophic balance (Holt and Thorpe 1991).

* Corresponding author: Joint Centre for Mesoscale Meteorology, Department of Meteorology, University of Reading, Earley Gate, PO Box 243, Reading, Berkshire RG6 6BB, UK. e-mail: k.a.browning@reading.ac.uk

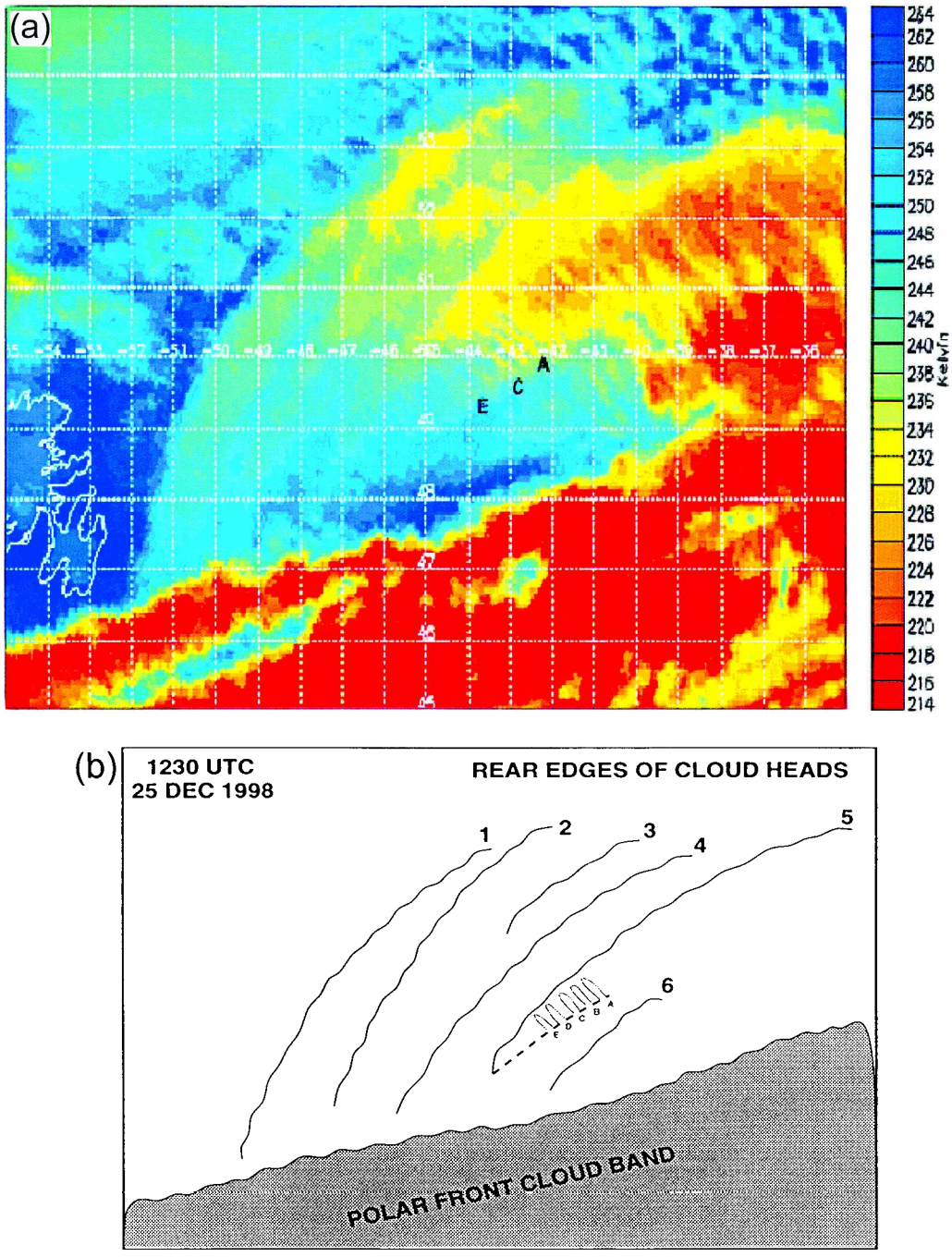

Figure 1. Meteosat infrared cloud image over the western North Atlantic showing multiple cloud heads with cloud-top striations at 1230 UTC 25 December 1998. (a) Colour-enhanced image (key gives brightness temperature in Kelvin) with three striations labelled (A, C, E). (b) Sketch of rear edges of the six partially overlapping cloud heads to the north of the polar-front cloud band, with several cloud-top striations (labelled A, B, C, D, E) behind a region of suspected line convection (dashed line) associated with Cloud Head 5. (c) Model-derived upper-air sounding for the region of the labelled cloud-top striations (each full barb = 5 m s^{-1}. Taken from Dixon *et al.* 2000).

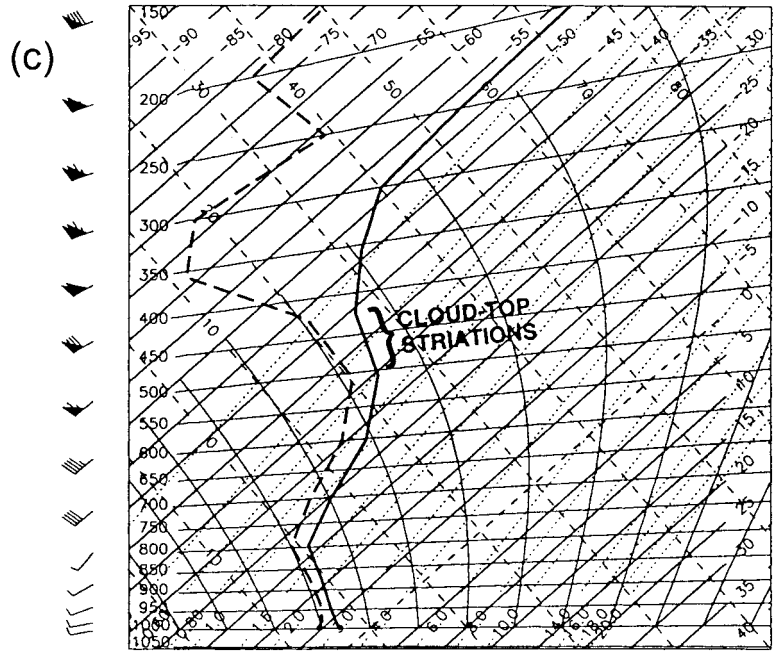

Figure 1. Continued.

Occasionally, in the case of vigorous ana-cold frontal circulations, a further mesoscale structure can be seen in the satellite imagery: this is the phenomenon of cloud-top striations, in which the tops of the clouds associated with the slantwise circulations are characterized by front-perpendicular striations in cloud-top height. Many cases of such striations have been observed in Australia by Feren (1995) who regarded them as an indication of strong winds and rapid deepening; of the 37 lows that exhibited what Feren called a 'striated delta' cloud structure, 75% were associated with at least gale force winds and most exhibited a 12-hour period of explosive deepening. A recent example of cloud-top striations over the North Atlantic is shown in Fig. 1(a) which is a single frame from the animated sequence of colour-enhanced Meteosat infra-red images that Dixon *et al.* (2000) showed in their electronic-journal article. Figure 1(b) is their sketch of the salient features. They suggested that multiple slantwise convective circulations led to the six partially overlapping cloud features referred to in the figure as cloud heads; line convection may have been occurring along the inner edge of some of the cloud heads, as shown for Cloud Head 5. The cloud-top striations have a wavelength of 30 to 55 km, and in the case of Cloud Head 5 they extend from the position of the line convection at the leading edge towards the rear edge of the corresponding cloud head. The region of striations extends north-eastwards within Cloud Head 5 far beyond the region occupied by the striations labelled A to E. Cloud Head 6 also shows evidence of cloud-top striations.

Dixon *et al.* (2000) attributed the cloud-top striations in Fig. 1(a) to upper-level convection. The model-derived sounding in Fig. 1(c) indicates a more nearly neutral lapse rate (compared with adjacent layers) between 500 and 420 mb which may have been associated with the striations. Unfortunately the event they studied occurred over the sea without any direct ground-based observations and so their conclusions were tentative. Since then we have been looking for similar events to occur over land where

they can more easily be observed by radars. Although such events occur less frequently over land in north-west Europe than over the Atlantic, such occurrences were detected by satellite over the UK in association with intense ana-cold fronts on 5 November 1999 and 30 October 2000. In both cases the circulations were associated with what R. B. Weldon called baroclinic cloud leaves, or simply cloud leaves (see Bader *et al.* 1995, p. 121), rather than with cloud heads (Bader *et al.* 1995, chapter 5); the two kinds of cloud feature are similar, however, in that both are associated with strong ana-cold frontal circulations. We present observational case-studies of these two events in this paper. The 30 October case, presented briefly in section 2, was associated with a very rapidly deepening cyclone which produced severe gales and heavy rain. This is followed in section 3 by a more thorough analysis of the 5 November case which was more notable for the associated heavy rain than for the intensity of cyclogenesis (10 mb in 12 hours). The studies support the hypothesis that the cloud-top striations detected in the satellite imagery are due to upright convection initiated at the top of vigorous rearward-sloping slantwise convection.

The main sources of mesoscale information used to interpret the satellite-detected cloud-top striations are: (i) non-standard high-resolution analyses of data from the operational ultra high frequency (UHF) wind-profiler radars operated by the Met Office at Pendine on the South Wales coast and at Camborne in south-west England; (ii) the very high frequency (VHF) Mesosphere–Stratosphere–Troposphere (MST) radar at Aberystwyth on the west coast of Wales (Slater *et al.* 1991); (iii) the high-resolution S-Band Doppler radar at Chilbolton in central southern England (Goddard *et al.* 1994); and (iv) the routinely available data from the UK weather radar network. Locations of the specialized radars are plotted in later figures as appropriate. Data are also used from a well-placed radiosonde at Aberporth near the Aberystwyth radar and from an operational run of the mesoscale version of the Met Office Unified Model.

2. Brief case-study of the cloud-top striations on 30 October 2000

The Meteosat infrared images in Fig. 2 show consecutive views of cloud-top striations associated with a baroclinic cloud leaf developing in the 'dry slot' region close to, and just south of, the centre of a low that was undergoing very rapid cyclogenesis. The striations have an average wavelength of about 35 km and are situated on top of, and orientated roughly at right angles to, the cloud leaf the boundaries of which are shown by the two black lines in Fig. 2(a). Individual striations are labelled A to H, of which the first six are identified in both images; they were travelling north-eastwards at 47 m s^{-1}.

The cloud-top striations passed directly over the UHF wind-profiling radar at Pendine on the south coast of Wales (situated beneath the letter C in Fig. 2(a)). The positions of all the letters A to H correspond to the parts of each striation that are estimated to have passed over the Pendine radar. These same features are also identified in the Pendine time–height reflectivity plot in Fig. 3(a), which shows a reasonable correspondence between the satellite-observed striations and the series of rather regularly spaced echo columns at the top of the main area of echo. This radar obtains returns both from refractive-index fluctuations in the clear air and from precipitation, but almost all of the echo above 3 to 4 km is from precipitation. The columnar nature of these upper-level echoes and their intensity are indicative of fairly vigorous upright convective cells. These are seen to be extending vertically between 5 and 8 km in the case of striations A to D (less for E to H).

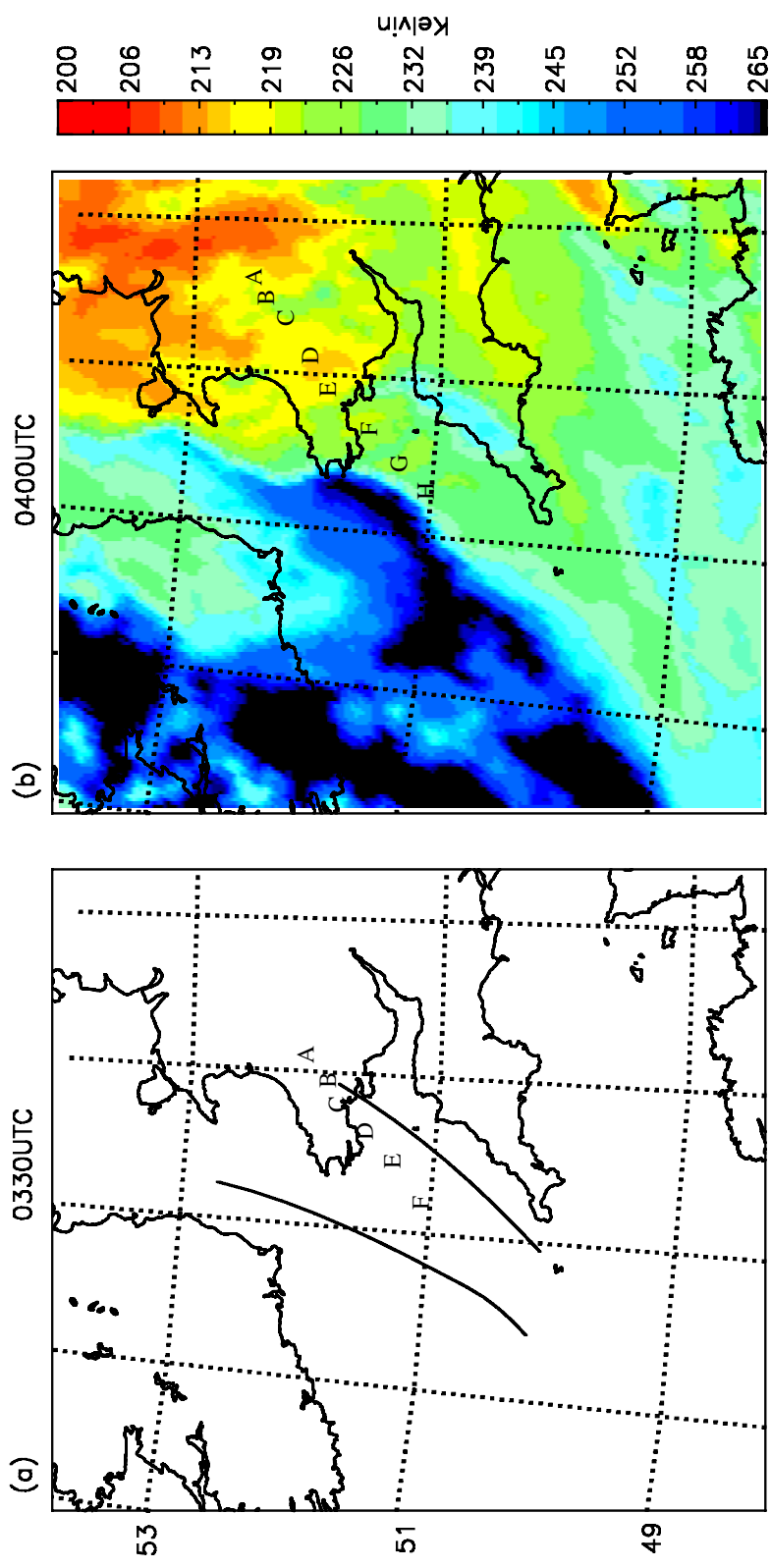

Figure 2. Colour-enhanced Meteosat infrared cloud images at (a) 0330 UTC, and (b) 0400 UTC on 30 October 2000, showing a cloud leaf, with cloud-top striations (A–H), extending from west of Cornwall to south-west Wales (between the two black lines in (a)).

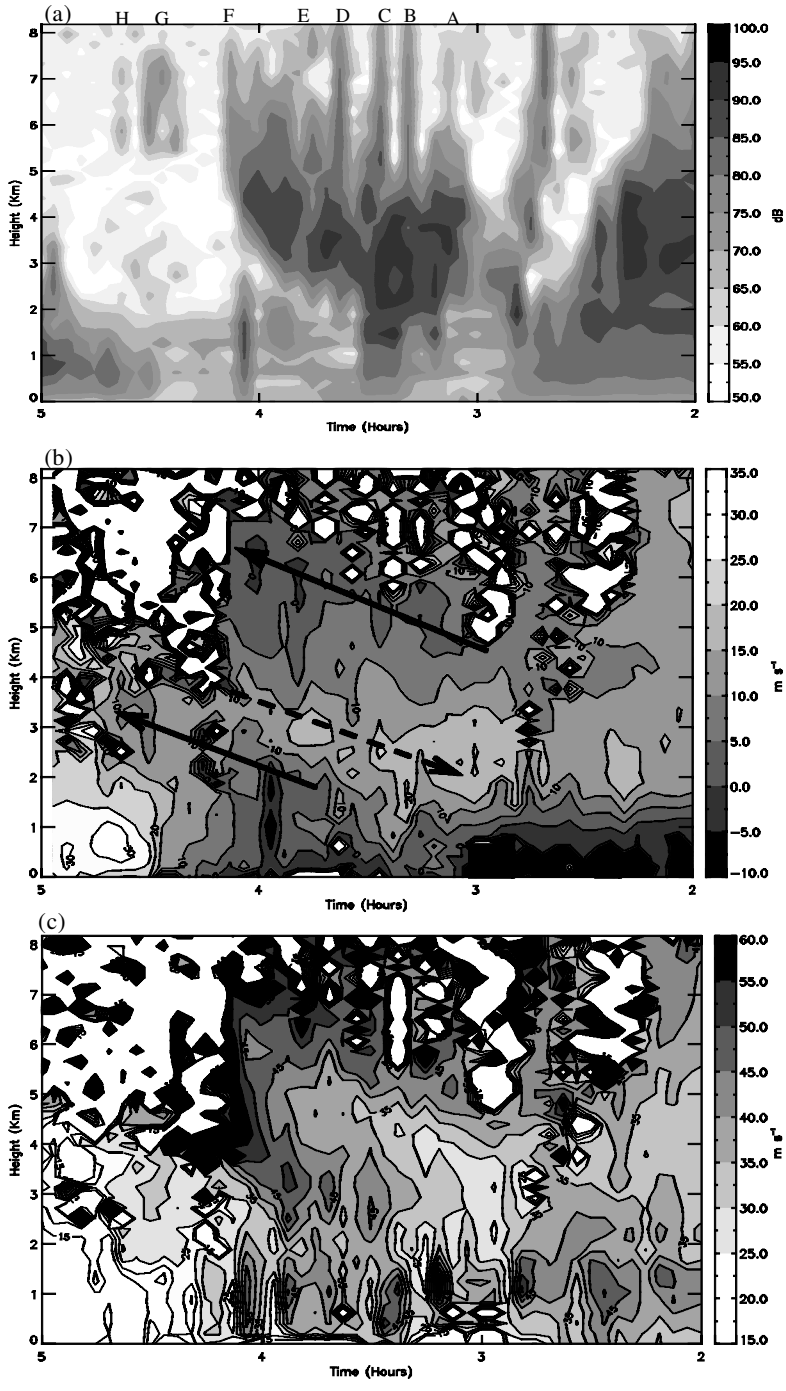

Figure 3. Time–height plots at high temporal resolution (3.5 minutes) of: (a) received power (dB), (b) front-perpendicular wind component (m s^{-1}), and (c) front-parallel wind component, as measured by the UHF radar at Pendine between 0200 and 0500 UTC 30 October 2000. The positions of cloud-top striations A to H are indicated in (a). Arrows in (b) represent axes of transverse circulations as explained in the text. Speckled areas of shading in (b) and (c), mostly at high levels, show where the reflectivity is too weak to enable velocity measurements to be made.

Figure 3(b)* shows the time–height distribution of the component of the wind perpendicular to the front. The frontal orientation is taken as 220 to 040°. Winds overtaking the frontal system (from left to right) are shown as lightly shaded areas (except in places at high levels where white areas are due to low signal-to-noise). The frontal system was travelling at almost 10 m s^{-1} normal to the axis of the front and so the darkly shaded areas represent rearward-directed flows relative to the system. The rearward-directed flow depicted by the inclined solid arrow in the lower left-hand corner of the diagram corresponds to an ascending flow feeding a cloud head located behind (to the west of) the cloud leaf. The upper two inclined arrows in this figure represent the transverse circulation associated with the cloud leaf itself. The circulation is quite deep and strong; the difference in speed between the maximum rearward-directed flow (solid arrow) and the maximum forward-directed flow (dashed arrow) is almost 20 m s^{-1}.

Comparison of Fig. 3(b) with Fig. 3(a) shows that the dashed arrow representing the maximum forward-directed component descends at the base of an inclined layer of precipitation echo, beneath which the reflectivity decreases rapidly due to the evaporation of the ice particles as they descend into a dry layer. This is consistent with the dashed arrow being FSD. Analysis of the mesoscale model output (not shown) demonstrates that this was a dry-intrusion flow associated with a major tropopause fold. Conversely, the uppermost solid arrow representing the maximum rearward-directed wind component in the cloud leaf is seen to be in a region where reflectivity increases downwards (Fig. 3(a)), indicating that this flow corresponds to RSA responsible for the growth of precipitation. It is possible that the RSA flow was being fed in part and intermittently by upright convection of air from the boundary layer, but there is no clear signature of line convection in Fig. 3 (although there is a hint in Fig. 3(b) of convergence (strictly confluence) in the lowest 1 km at 0300 UTC with overlying divergence (diffluence) at 5 km).

From the perspective of what might have been responsible for the cloud-top striations, it is significant that the uppermost solid arrow in Fig. 3(b), representing the maximum in rearward-directed velocity (about 0 m s^{-1} relative to the ground), is situated close to the base of the convective echo columns in Fig. 3(a). In accordance with the ideas of Bennetts and Hoskins (1979), it is the local maximum in rearward-directed flow in the slantwise convection that probably leads to a buckling of the wet-bulb potential temperature (θ_w) surfaces, and to the potential instability and upper-level convective cells. Figure 3(c) shows that the front-parallel wind component at and above the level of the uppermost solid arrow in Fig. 3(b) is between 45 and 50 m s^{-1}, close to the 47 m s^{-1} speed of travel of the striations as estimated from the full sequence of satellite images like those in Fig. 2. This is consistent with the echo columns being due to upper-level convective cells advected with the winds above the RSA flow. It is not consistent with a gravity-wave hypothesis which would require the features to propagate relative to the flow at their level.

A similar picture emerges for the other case-study but the observational data show it more clearly. Therefore we shall examine the other case in more detail.

3. Case-study of the event of 5 November 1999

A developing cyclone travelled east-north-eastwards across Northern Ireland and southern Scotland during 5 November 1999. It produced large falls of rain over many

* In Figs. 3(b) and (c), and in Figs. 7(a) and (b), the high degree of short-term wind variability at low levels may be an artefact, and does not significantly affect interpretations in this paper.

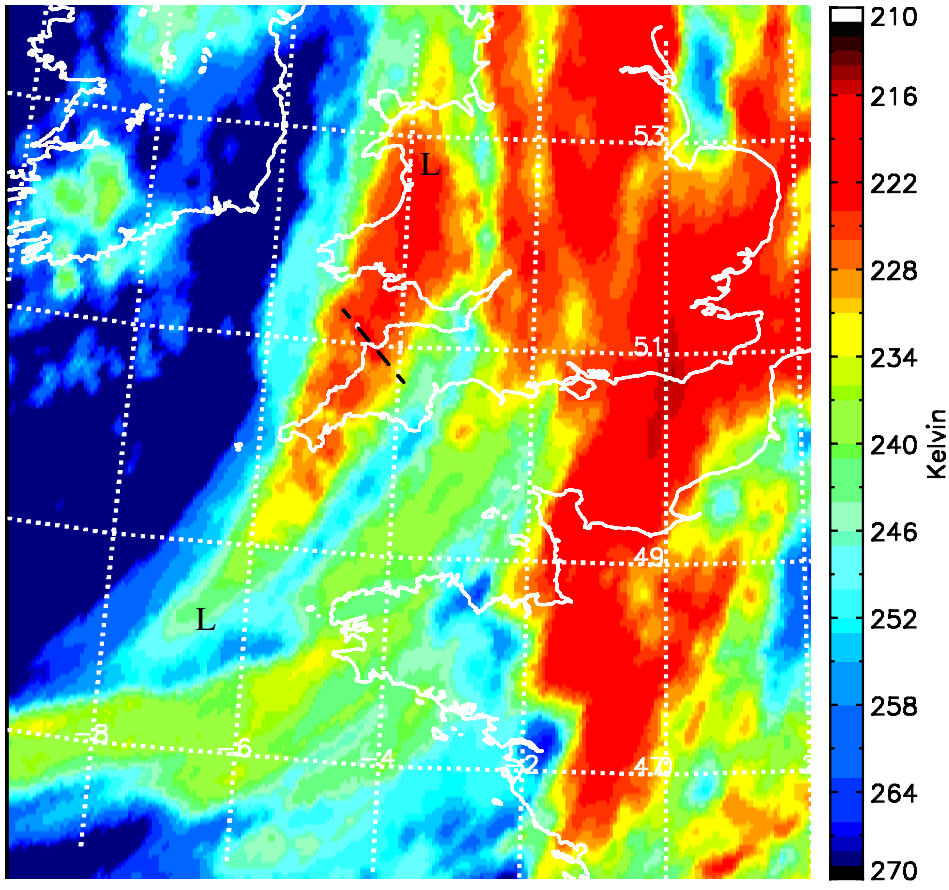

Figure 4. Colour-enhanced Meteosat infrared cloud image at 1000 UTC on 5 November 1999, showing a cloud leaf (LL), with cloud-top striations, extending from west of Brittany to north Wales. The axis of one of the striations (Striation T in Fig. 9) is highlighted by a dashed line.

parts of the British Isles and moderately strong winds. Between 0000 and 1200 UTC it deepened from 994 to 984 mb. The cloud-top striations on this occasion were associated with an ana-cold front which extended to the south of the low. The Meteosat infrared image in Fig. 4 shows that the cloud-top striations at 1000 UTC were within a well-defined cloud leaf which was associated with the ana-cold front as it travelled eastwards across Wales and south-west England. The cloud-leaf (labelled LL) is the region of high (cold) cloud situated towards the rear edge of the overall region of frontal cloudiness, associated with the main cold-frontal zone. The western edge of the high cloud associated with the cloud leaf corresponds to the axis of the upper-level jet. The eastern edge of the cloud leaf is close to the SCF. The striations are seen to be orientated north-west to south-east. Tops are higher in the striations over the coast of South Wales and lower in the striations to the south-west of England.

(*a*) *The synoptic context*

The surface analysis at 1100 UTC (Fig. 5(a)), obtained from the mesoscale version of the Met Office's operational Unified Model, shows the developing cyclone over central Scotland, with a frontal fracture as described by Shapiro and Keyser (1990). The cloud

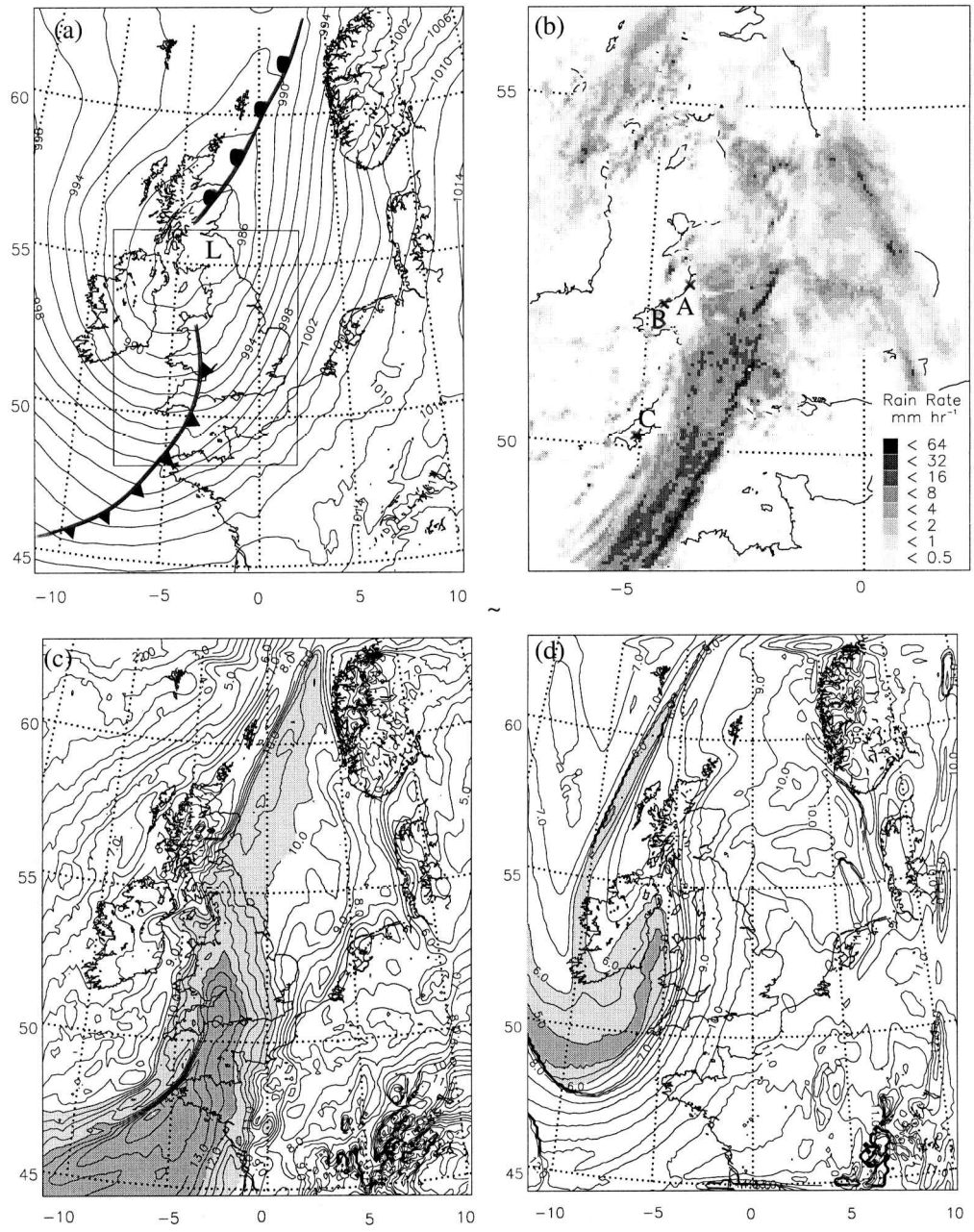

Figure 5. Structure of the frontal system in plan view at 1100 UTC 5 November 1999 as derived from the T+5 hour forecast from the operational mesoscale model. (a) Mean-sea-level pressure (mb) and frontal analysis. (b) Radar rainfall distribution within the inner rectangle in (a); crosses A, B and C denote the locations of Aberystwyth, Aberporth and Camborne. (c) Wet-bulb potential temperature at 900 mb with contours at 0.5 degC intervals (shaded lightly and more heavily for $\theta_w > 10$ and 12 °C, respectively). (d) Height of the dynamic tropopause (potential vorticity = 2 PV units) with contours at 0.5 km intervals (shaded lightly and more heavily for heights below 6.0 and 5.0 km, respectively). Distorted contours near the domain boundary are an artefact of the model.

leaf shown in Fig. 4 was associated with the cold front extending from the English Midlands to Brittany. The radar-network display covering the boxed area in Fig. 5(a) shows a WCFR 100 km wide with an intense NCFR at its leading edge (Fig. 5(b)). The rear edge of the WCFR is parallel to the axis of the upper-level jet (shown in later vertical sections) and this was fractured in the same way as the associated fronts. The θ_w distribution at 900 mb (Fig. 5(c)) shows that the cold front associated with the primary NCFR was sharp, with a step change of about 4 degC over the English Channel. Behind the cold front there was a deep intrusion of stratospheric air; Fig. 5(d) shows the dynamic tropopause (potential vorticity $(PV) = 2$ PVU*) descending below 5 km.

Figure 6 shows time–height sections at Aberystwyth (location A in Fig. 5(b)) for the entire day on 5 November 1999. Figures 6(a) and (b) are from the VHF radar and show u and v components of the wind perpendicular and parallel to the cold front, respectively. Figure 6(c) is a corresponding section showing θ_w, v and $PV = 1$, derived from the nearest grid point of the mesoscale model. The passage of the upper-level jet shows up clearly in the v component from both the radar (Fig. 6(b)) and the model (Fig. 6(c)); peak values are close to 50 m s^{-1} in both cases, although the model shows it two hours too early. The striated cloud leaf passed over Aberystwyth between 0800 and 1200 UTC. As shown later, the tops of the cloud leaf correspond in height to the top of the moist shaded area in Fig. 6(c) provided allowance is made for the two-hour error in the model.

Figure 6(a) shows three layers of maximum front-perpendicular wind-component within the troposphere below 7 km: S1, S2 and S3. They are inclined upwards towards the left, i.e. to the rear side of the frontal system as it travelled from left (west) to right (east). Layers S1 and S2 were within the cloud leaf and layer S3 was just behind it. These layers are similar to the layers analysed by Browning *et al.* (2001a), i.e. they correspond to their stacked multiple layers of slantwise convection, or RSA in the terminology of the present paper. Comparison between Figs. 6(a) and (c) shows that all the layers of slantwise convection were within the strongly baroclinic zone beneath the main upper jet, and that they extended towards the region of a major tropopause depression characterized by the $PV = 1$ boundary. High PV is also seen at lower levels in the region of S1 and S2 but this was a mainly saturated region and the PV was diabatically generated. The model did not represent the individual circulations S1 and S2, probably because of its inadequate resolution (12 km horizontal grid and 38 levels in the vertical).

The VHF radar at Aberystwyth cannot make measurements in the lowest 1.8 km and so we use other observations to investigate the relationship of the layers of slantwise convection to line convection in the boundary layer. Fortunately the cloud leaf also passed over the UHF radars at Camborne and Pendine, both of which can provide measurements close to the ground, albeit with poorer high-altitude performance. Here we present the results from just the Camborne radar (location C in Fig. 5(b)).

Time–height records of the received power and of the u and v components of the wind as measured by the Camborne UHF radar are shown in Figs. 7(a), (b) and (c), respectively. In Fig. 7(b), one can see layered perturbations in the u component sloping predominantly upwards towards the left. The system velocity defined by the motion of the SCF corresponded to a u component of about 11 m s^{-1}, from which it can be seen that there is a well-defined RSA flow, highlighted by the arrow labelled S1, which appears to be fed by line convection at L1. Beneath S1, and perhaps characterized by a slightly faster system velocity, there are two weaker RSA flows, S2a and S2b, separated in the vertical by 2 km. These correspond to substructure of the flow labelled S2 in the

* PV is given in Potential Vorticity Units (PVU); 1 PVU $= 10^{-6}$ K $m^2 kg^{-1} s^{-1}$.

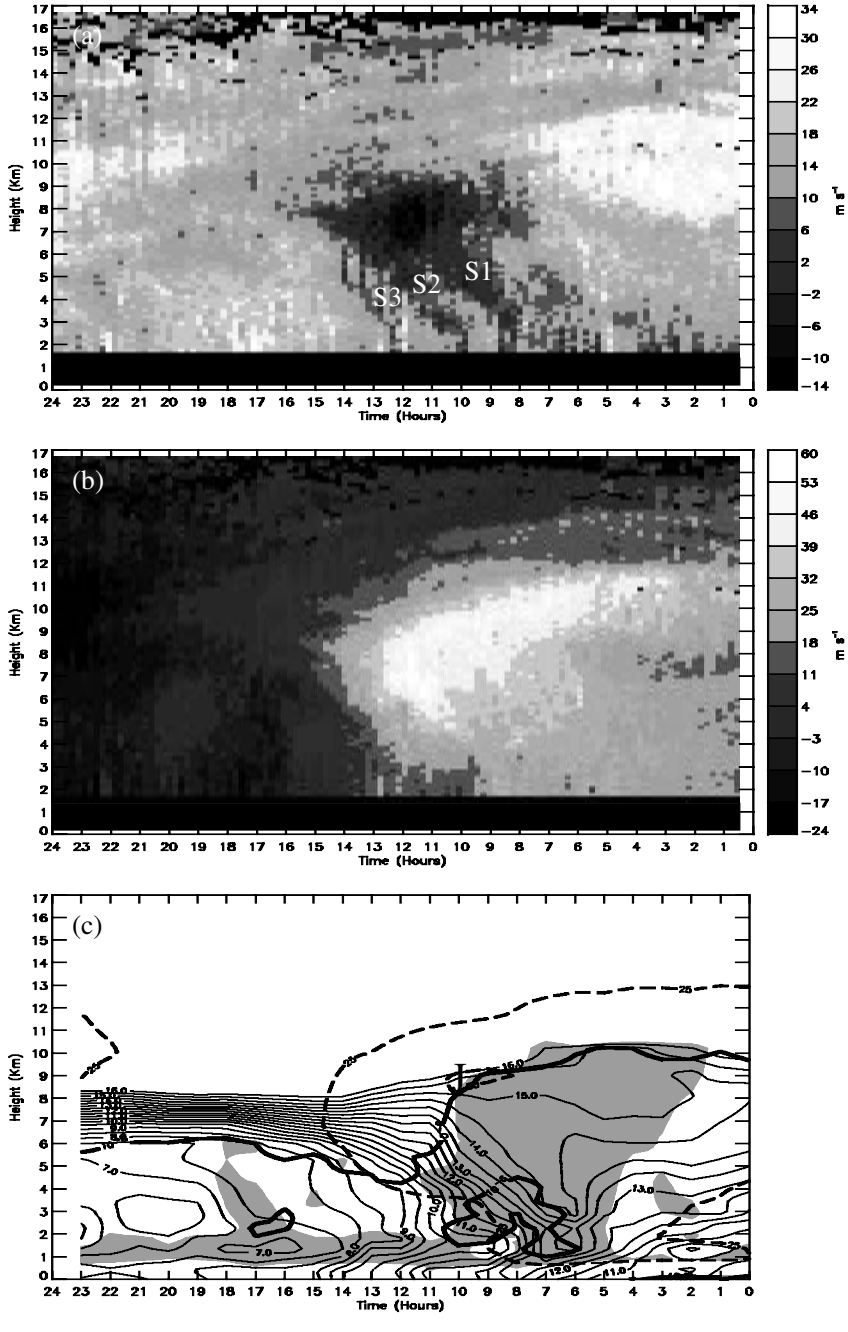

Figure 6. Structure of frontal system as seen in time–height sections at Aberystwyth (see Fig. 5(b)) over 24 hours on 5 November 1999. The cloud leaf with cloud-top striations passed overhead between 0800 and 1200 UTC. Panels (a) and (b) are from the VHF radar and show wind components perpendicular and parallel to the front, respectively. The velocity of the frontal system was 11 m s^{-1} and dark colours in (a) correspond to front-to-rear relative flows, three of which are labelled S1, S2 and S3. (S2 has substructure which is identified as S2a and S2b in Figs. 7(b) and 13.) (c) Shows a synthesis of information from the mesoscale model: the solid contours show wet-bulb potential temperature at 0.5 degC intervals, the dashed contours show front-parallel wind components of 25 and 50 m s^{-1} (J at the centre of the 50 m s^{-1} contour denotes the upper-level jet), the thick solid line denotes potential vorticity = 1 PV unit, and the shaded area is where relative humidity with respect to ice exceeds 99%.

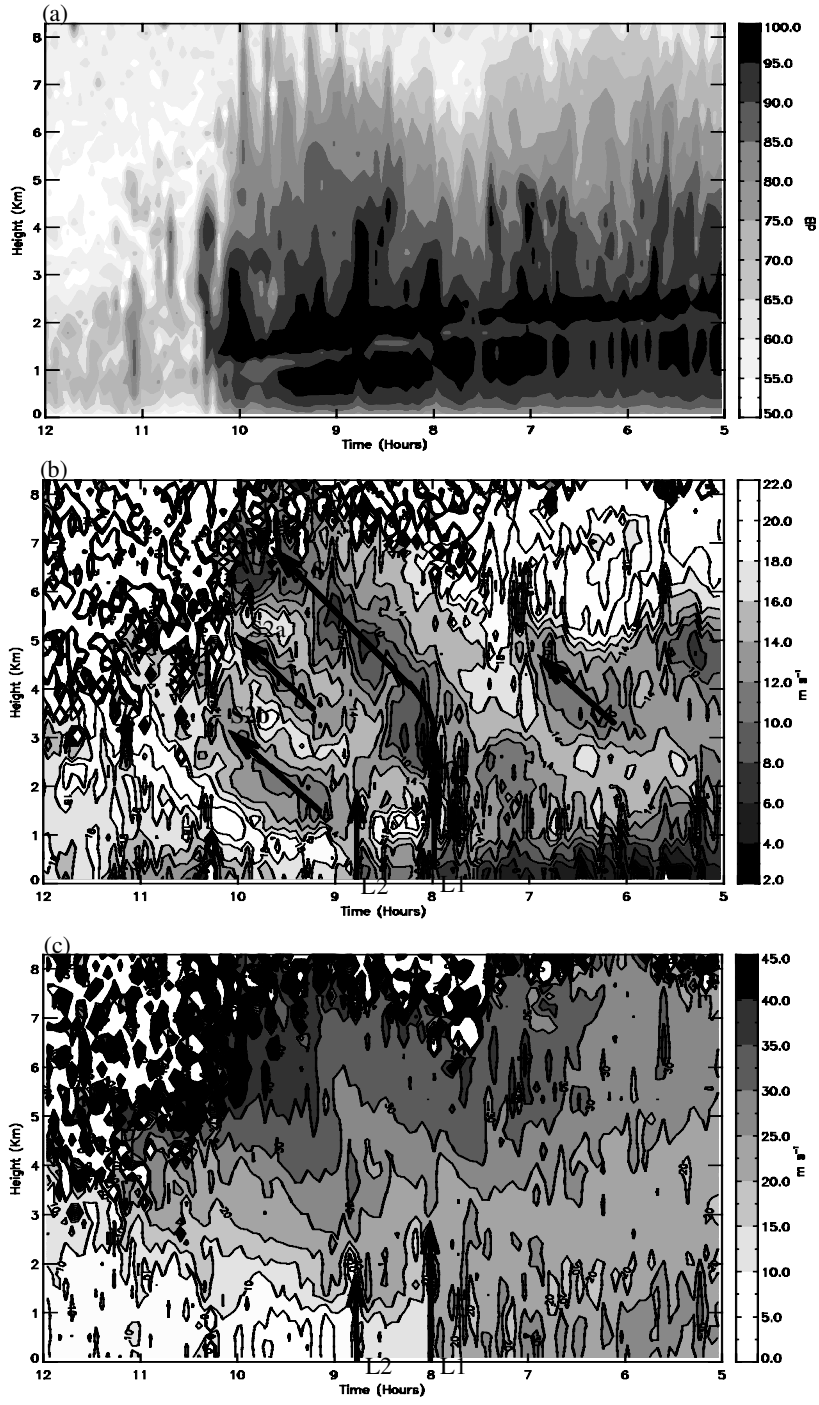

Figure 7. Time–height plots of: (a) received power (dB), (b) front-perpendicular wind component (m s^{-1}), and (c) front-parallel wind component, as measured with the UHF radar at Camborne between 0500 and 1200 UTC 5 November 1999. The striated cloud leaf passed overhead between 0800 and 1000 UTC. The superimposed inclined arrows denote front-to-rear relative flows: the strongest such flow corresponds to S1, also shown in Fig. 6(a). The two layers labelled S2a and S2b correspond to the layer labelled S2 in Fig. 6(a). The vertical arrows L1 and L2 represent line-convection features which were related to S1 and S2 (S2a + S2b), respectively.

Aberystwyth section in Fig. 6(a). They appear to be associated, more loosely, with line convection at L2. Other weak RSA flows can also be seen to have existed before the arrival of L1. The various RSA flows were separated by shallow FSD flows (white or very pale shading in Fig. 7(b)), the strongest one entering the rear of the system at 3 km at 1100 UTC and descending to 1.2 km at 1000 UTC and 600 m at 0900 UTC.

The measurements in Figs. 7(b) and (c) show the abrupt wind changes at low levels that accompanied the passage of line convection, L1 at 0800 UTC and, to a lesser extent, L2 at 0845 UTC. In Fig. 7(c), v in the lowest 2 km decreases from over 25 to under 15 m s^{-1} during the passage of the primary line convection, L1. This would correspond to a cyclonic shear of 10^{-2} s^{-1} assuming the change took place within 1 km. Referring to Fig. 7(b), it can be seen that the u component in the lowest few hundred metres increases from 8 to 12 m s^{-1} during the passage of L1 (albeit in two stages owing to the fine structure along the line convection). Directly above this low-level confluence there is a corresponding region of diffluence at 3 km, consistent with the shallow upright convection L1, as shown by the near-vertical arrow. A further region of low-level confluence, associated with an increase in the u component, from 12 to 16 m s^{-1} occurs at L2, with a region of diffluence above it between 1.5 and 2 km, consistent with the even shallower upright convection in this region.

As is sometimes seen at line convection (e.g. Browning and Harrold 1970), a region of low v component (pale shading in Fig. 7(c)) extends upwards as a narrow tongue just on the cold-air side of line convection, L1. The resulting deficit in momentum in the upper parts of the line convection is presumed to be a result of the upward transport of some of the low-momentum cold air alongside the warm air ascending at the SCF. A similar but shallower v perturbation can be seen at 0845 UTC in association with the weaker line convection, L2.

The power plot in Fig. 7(a) shows abundant echo from precipitation extending to high levels until just after 1000 UTC, following which the echo is mainly from the clear air. The intense layer echo sloping down from 2.4 to 1.4 km is associated with the melting layer which lowers during the passage of the cold-frontal zone. The superimposed vertical streakiness is caused by inhomogeneities in precipitation intensity which are believed to be at least partly due to the precipitation originating in upper-level convective generator cells (cf. our analysis of Fig. 3(a)). Probably the strongest upper-level convective cells would have been associated with the intense echo columns in and above the RSA flow S1, from 6 to above 8 km between 0900 and 1000 UTC. These occurred during the passage of the cloud-top striations, as shown by Fig. 4.

(*b*) *Interpretation of the cloud-top striations*

We now focus more closely on the mechanism of the cloud-top striations associated with the cloud leaf. The colour-enhanced infrared satellite image in Fig. 4 shows that the striations, with a wavelength of about 50 km and orientated roughly transverse to the axis of the cloud leaf, have brightness temperatures over the range 220 to 235 K. Assuming an emissivity of unity, this corresponds to cloud tops between 8 and 10 km, i.e. close to tropopause level in the vicinity of the upper-level jet (J) shown in Fig. 6(c). As discussed in subsection 3(a), the cloud-top striations were situated above multi-layered slantwise circulations that were being fed in part by line convection from the boundary layer. The strongest of these circulations was associated with the intense line convection, L1, at the SCF which fed the RSA feature labelled S1 in Figs. 6 and 7. As noted above in connection with Fig. 7(a), the upper parts of the radar echo, above 6 km, consisted of

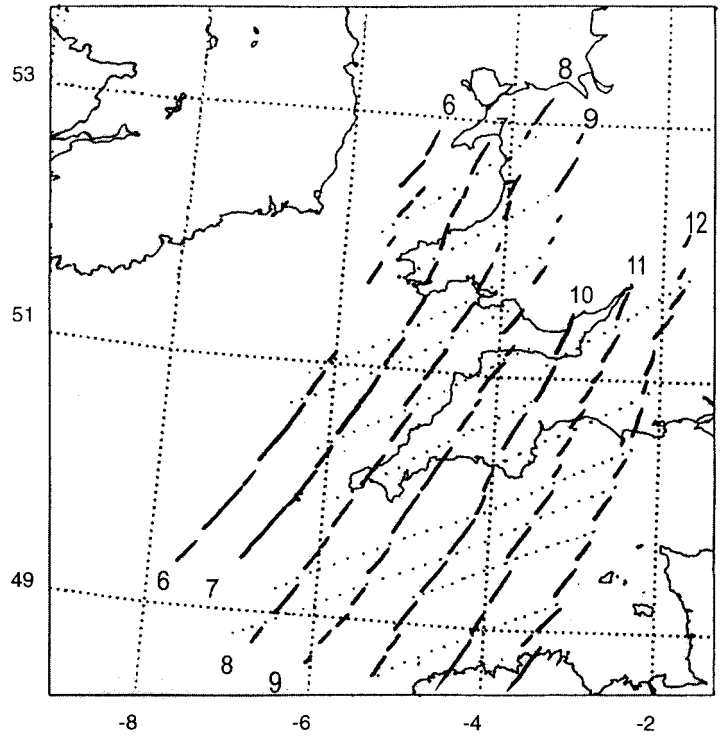

Figure 8. Tracings of line-convection elements (solid lines) at one-hour intervals from 0600 to 1200 UTC 5 November 1999, and the tracks of the gaps between them (dotted lines) as derived from the weather radar network pictures.

separate echo columns (as for the previous case-study in section 2), thereby suggesting the presence of upper-level convective cells above S1. A convective origin for the cloud-top striations was in fact proposed by Dixon *et al.* (2000); however, this was one of several hypotheses that they proposed and we shall now examine them in turn.

(i) *Hypothesis 1: Plumes from individual elements of line convection.* Line convection at the SCF contributes to some (not all) of the RSA. Line convection is broken into elements with a range of scales both comparable to and smaller than the wavelength of the cloud-top striations, and so one of the hypotheses proposed by Dixon *et al.* is that the striations are related to the plumes emanating from individual (or aggregates of) line-convection elements. To test this hypothesis we consider the velocity of travel of one of the striations, shown dashed in Fig. 4 and referred to as Striation T elsewhere, and we relate it to the motion of a nearby line-convection element.

Figure 8 shows tracings of the successive hourly positions of line elements associated with the main line convection, L1, as derived from weather radar network pictures, like that in Fig. 5(b), available at 15-minute intervals. The direction of travel of the line elements is shown by the dotted lines which connect successive positions of the gaps between the line elements. In reality there were more gaps than shown here because the 5 km resolution of the radar network data does not resolve some of the smaller gaps. However, for the purpose of the present analysis what matters is their velocity of travel.

Figure 9 shows successive half-hourly positions of Striation T from 0830 to 1200 UTC. For each time in Fig. 9 the axis of Striation T is extended (dashed lines)

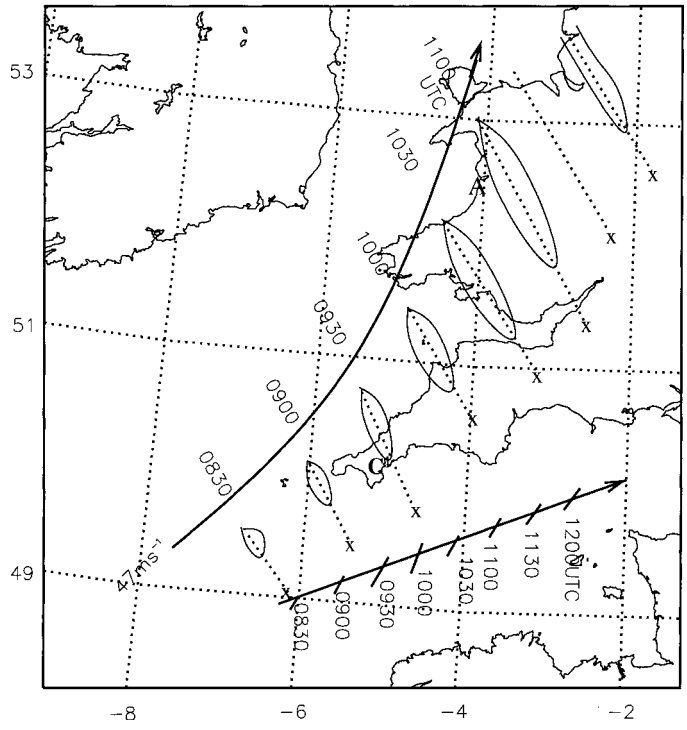

Figure 9. Successive half-hourly positions of cloud-top striation T (contours) between 0830 and 1100 UTC 5 November 1999, as determined from the Meteosat infrared images. The dashed lines along the axis of the striation are terminated where they intersect the position (X) of the line convection along the surface cold front. Successive positions of the individual line element that is intersected at 0830 UTC are also plotted. A and C denote the locations of the VHF and UHF radars at Aberystwyth and Camborne, respectively.

to the location (X) of the line convection at the corresponding time. Separately, Fig. 9 also shows the successive half-hourly positions of the particular line-convection element that was nearest to Striation T at 0830 UTC, as obtained from Fig. 8. It is clear that the track of this line element is quite different from that of the end of Striation T closest to the line convection, thereby disproving the hypothesis of a one-to-one link between striations and individual line elements as source regions for plumes.

(ii) *Hypothesis 2: Gravity waves.* The location, orientation, and characteristic scale of the striations are broadly consistent with the hypothesis that these features are associated with gravity waves. Specifically, the striations are located on the cold side of the surface front, in the inflection point downstream of a deep and sharply curved upper-level trough, and near the exit region of an upper-level jet streak. Such an environment has been widely hypothesized (e.g. Koch and O'Handley 1997) as being conducive to the breakdown of dynamical balance and the process of geostrophic adjustment (where it is understood that the balanced state to which the flow is adjusting is not necessarily geostrophic; this process is also sometimes referred to as 'spontaneous adjustment emission' or 'Lighthill radiation'). Hence there would appear to be some circumstantial evidence for the possibility that the striations are associated with gravity waves generated by the breakdown of balance in the vicinity of the upper-level jet. This mechanism was favoured by Feren (1995).

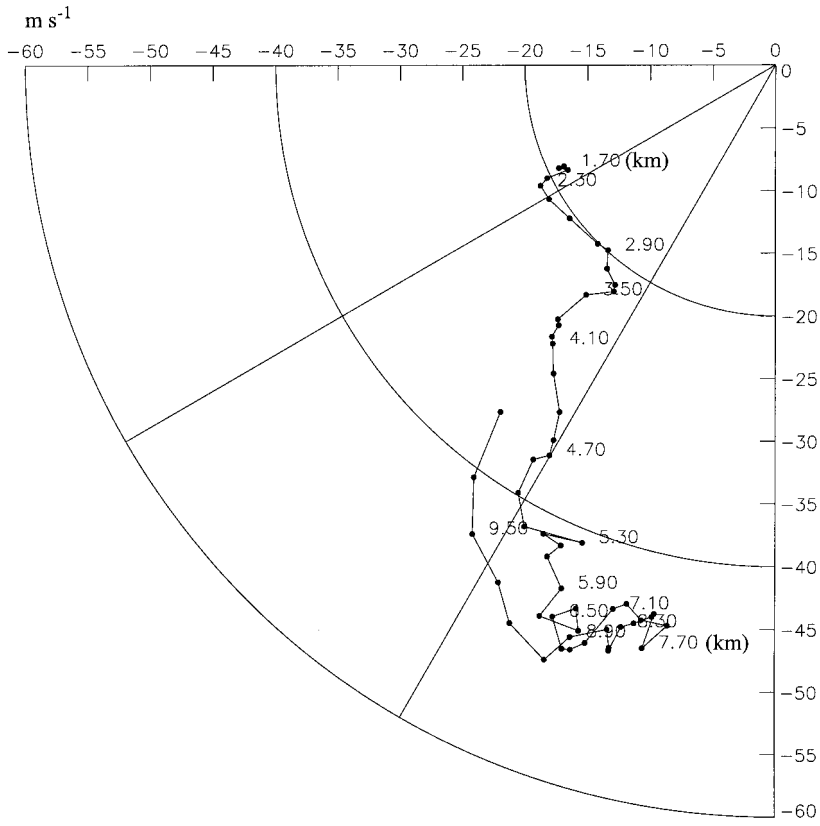

Figure 10. Wind hodograph derived from the VHF radar at Aberystwyth during the passage of Striation T (see text) between 1045 and 1100 UTC 5 November 1999. Winds are plotted at height intervals of 0.15 km.

To test the hypothesis that the cloud-top striations in the present study might be due to gravity waves we examine their propagation velocity in relation to the environmental winds in their vicinity. Figure 10 is a wind hodograph derived from the VHF radar at Aberystwyth (location A in Fig. 9) as Striation T passed overhead. This shows that the winds close to the cloud top reach a maximum between 8 and 9 km, close to the observed propagation velocity of the striations, 47 m s^{-1} from 195°. This tendency for the cloud-top striations to travel *with* the winds at their level was also observed in the case-study in section 2, and it argues against the gravity-wave hypothesis. (P. Cunningham (personal communication) has suggested that it is still perhaps conceivable that gravity waves are being generated by adjustment processes in the vicinity of the jet stream (in which case the waves are often stationary with respect to the jet), and that these waves are responsible for subsequently initiating and organizing the convection at upper levels by creating regions of potential instability. If the convection becomes vigorous, then presumably it loses the propagation characteristics of the gravity waves that generated it and acts like a coherent structure advected by local winds.)

(iii) *Hypothesis 3: Conditional symmetric instability.* Bennetts and Hoskins (1979) showed that the mesoscale bands of ascent due to the release of CSI are orientated along the direction of the thermal wind. Browning *et al.* (2001a) identified CSI as a contributory cause of transverse cold-frontal circulations resembling the multiple

slantwise circulations observed here. Values of slantwise convective available potential energy along the cold-frontal zone were estimated from the mesoscale model to have been in excess of 1000 J kg^{-1} in the present case. However, it seems unlikely that the cloud-top striations, with their orthogonal orientation, can also be attributable to the CSI.

(iv) *Hypothesis 4: Kelvin-Helmholtz Instability (KHI).* The orientation of the cloud-top striations is arguably consistent with Kelvin-Helmholtz (KH) billows occurring within part of the underlying layer characterized by a roughly front-parallel (predominantly thermal wind) shear. Figure 10 shows that the appropriately sheared layer is situated mainly below 5 km, and so this hypothesis would need to invoke KH disturbances in this layer perturbing the flow in the overlying layer where the cloud-top striations were observed. In any case, however, KHI can be ruled out as a possible cause of the striations because of the long (~50 km) wavelength of the striations. KH billows of such a long wavelength have never been observed and would require shearing instability to have been released over a depth of many kilometres. For a sheared layer of thickness Δz, Miles and Howard (1964) give the fastest growing wavelength as $7.5\Delta z$, which would imply a layer 7 km thick in this case. According to the Doppler radar at Chilbolton, deep billows were not observed in this case.

(v) *Hypothesis 5: Convective rolls.* The mechanism preferred, on balance, by Dixon *et al.* (2000) to account for cloud-top striations was convective rolls in an unstable layer near the top of the frontal cloud. This view was arrived at in the light of somewhat equivocal evidence from satellite and numerical weather prediction (NWP) model data in the absence of direct observations. In the present case the structure of the atmosphere in the vicinity of the striations was probed not only by the VHF and UHF radars at Aberystwyth and Camborne, respectively, but also by a radiosonde from Aberporth and later by the Chilbolton Doppler radar. Data from all of these sources collectively strengthen the case for the cloud-top striations being due to upper-level convection.

Figure 11 shows RHI scans by the Chilbolton radar at two times during the passage of the cold-frontal precipitation; Figs. 11(a) and (b) were obtained by scanning perpendicularly to the front as it approached (from the left) at 11 m s^{-1}. The SCF is at 35 km range. The Doppler scan (Fig. 11(a)) shows that, ahead of the SCF, blue boundary-layer air was being overtaken by the front. At 35 km range there is region of low-level confluence (red to blue), overlain between 3 and 5 km by diffluence (blue to red), associated with the vigorous line convection, L1, that was responsible for the intense low-level echo shown red in Fig. 11(b). This line convection can be seen feeding the layer of RSA (blue) that reaches a height of 5 to 7 km at the left-hand (western) edge of the display. This is the layer of RSA referred to earlier as S1. (The weaker layer of RSA, S2, can be seen beneath it at 2 km between 70 and 95 km.) Figures 11(a) and (b) corroborate the airflow structures shown earlier in Figs. 6 and 7, but the main purpose for showing them is to provide a specific context for interpreting Figs. 11(c) and (d). These sections were obtained by scanning *parallel* to the front, i.e. at right angles to the sections in Figs. 11(a) and (b), 107 minutes after (a) and (b), during which time the frontal system will have travelled 70 km. In other words, assuming a steady state, the sections in (c) and (d) can be visualized as intersecting (a) and (b) at a range of 70 km. They are thus situated behind and roughly parallel to the SCF, and they are orientated obliquely through the cloud-top striations at a stage when the striations still existed but were becoming weaker and less well organized.

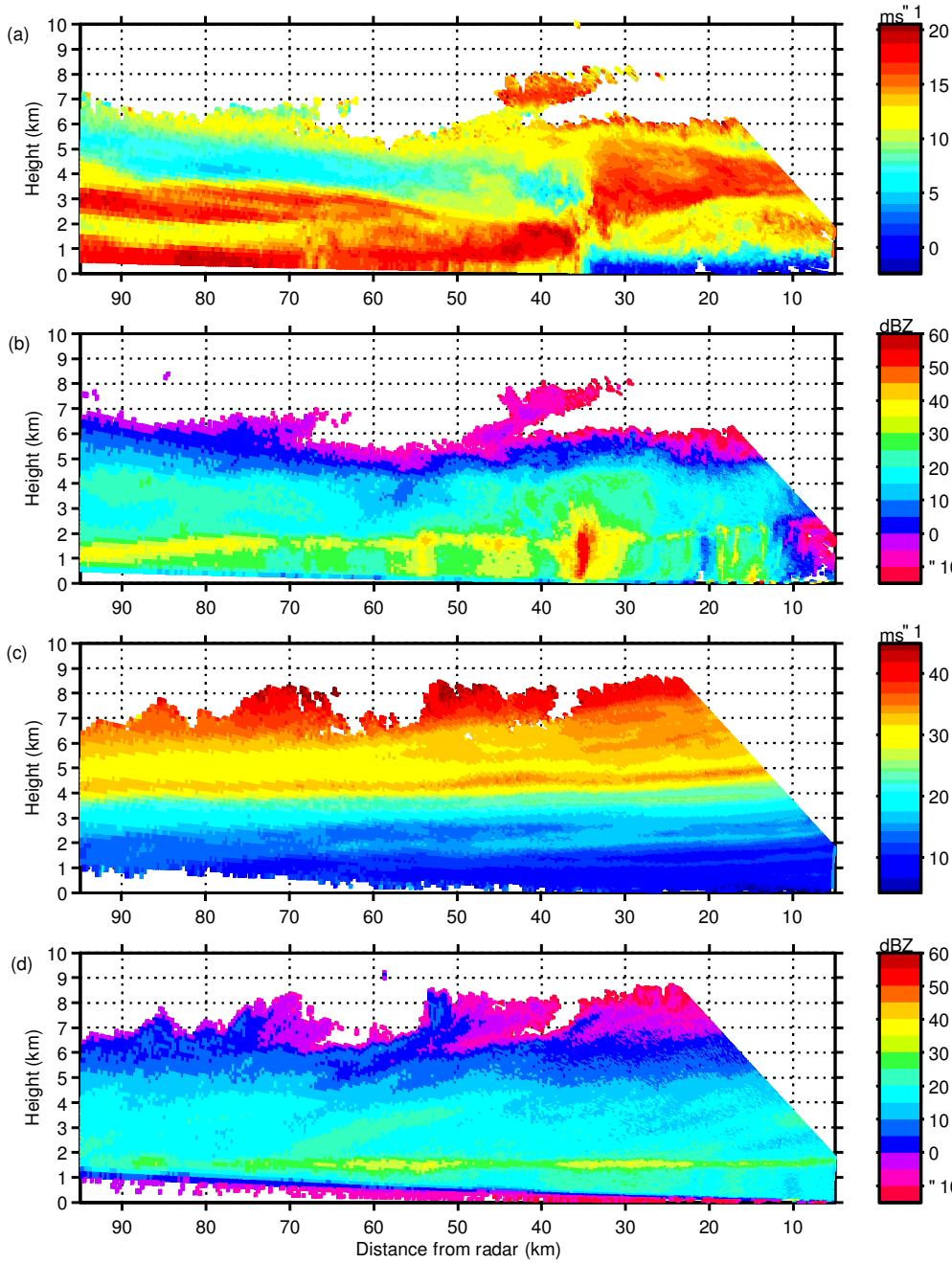

Figure 11. Vertical sections (RHI scans) as obtained with the Chilbolton microwave radar on 5 November 1999. Panels (a) and (c) show Doppler velocity in m s^{-1}; (b) and (d) show reflectivity in dBz. Panels (a) and (b) are at 1214 UTC; (c) and (d) are at 1401 UTC. The scan at 1214 UTC was obtained along azimuth 283°, roughly at right angles to the surface cold front (approaching from the left). The scan at 1401 UTC was obtained along 189° roughly parallel to the surface cold front.

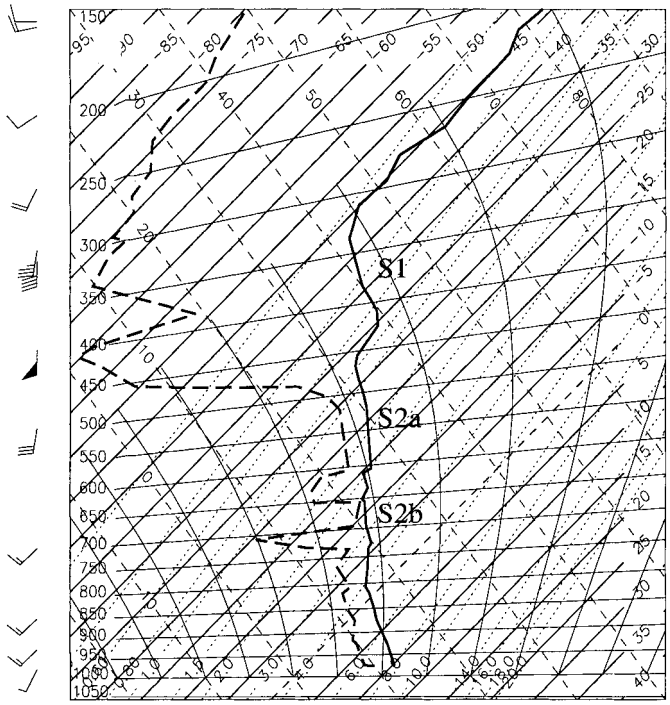

Figure 12. Tephigram for radiosondes released from Aberporth (see Fig. 5(b)) at 1100 UTC 5 November 1999. Solid line is temperature; dashed line is dew point. Three moist layers discussed in the text are labelled S1, S2a and S2b. Each wind barb corresponds to 10 m s^{-1} and a solid flag corresponds to 50 m s^{-1}.

Upper-level convection appears in Fig. 11(d) as clusters of upright columns of reflectivity (convective generator cells) between 7 and 8.5 km. (Recall the similar evidence of convective cells from the UHF radar reflectivity plots both for this case (Fig. 7(a)) and for the 30 October case (Fig. 3(a)).) The convective generator cells in Fig. 11(d) can be seen feeding strongly inclined ice-crystal streamers which, because of the strong thermal-wind shear below 6 km (cf. the wind hodograph in Fig. 10), reach the ground about 50 km south of the generator cells responsible for them. Figure 11(c) shows that the convective generator cells are themselves embedded within a layer in which the front-parallel component of the wind is only weakly increasing with height, i.e. they are (just) above the main layer of strong thermal-wind shear. The convective cells are occurring at the top of the strong RSA flows and are likely to be due to the release of potential instability generated by differential advection where the locally stronger front-normal flow within S1 (i.e. the strongly backed flow at 7.5 km in Fig. 10) leads to a buckling of the θ_w surfaces.

The most relevant thermodynamic sounding for this study is the 1100 UTC radiosonde ascent at Aberporth, shown in Fig. 12. This ascent was made at the rear edge of the cloud leaf and cloud-top striations. Figure 12 shows several moist layers, interspersed with drier layers, which can be related to the RSA flows previously identified as S1, S2a and S2b. Of particular interest is the near-neutral lapse-rate within the relatively moist, but not saturated, layer labelled S1. The sounding was, as already noted, made on the very edge of the cloud deck; within the main body of the cloud deck it is presumed that the layer S1 would indeed have been saturated and somewhat deeper, although probably still neutrally stratified owing to the ongoing release of the convective instability. A

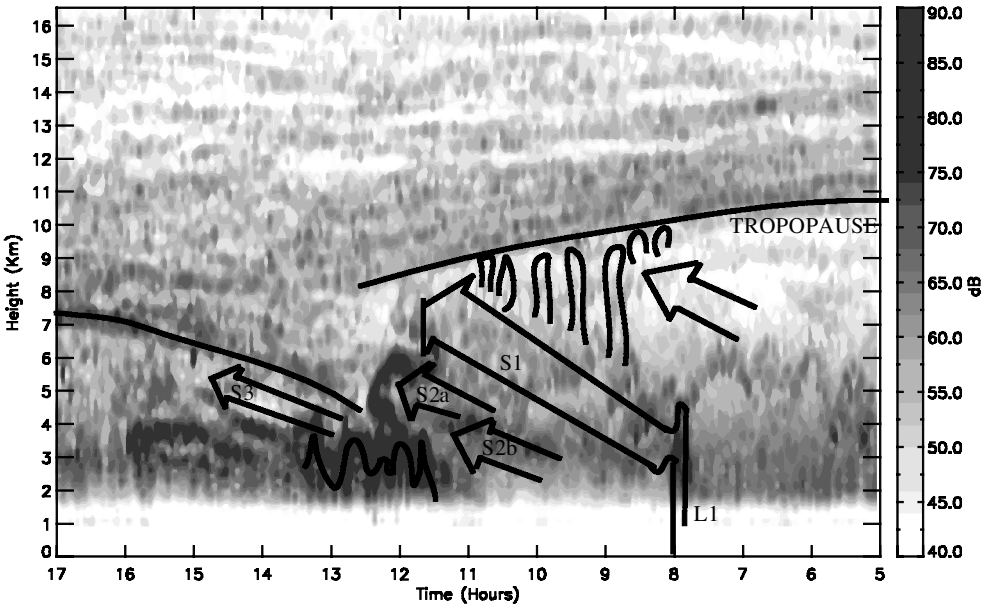

Figure 13. Simplified representation of the convective circulations associated with the intense ana-cold front, superimposed on the time–height plot of VHF radar echo power for 0500 to 1700 UTC 5 November 1999. Inclined arrows represent the rearward-sloping ascent part of the multiple slantwise convective circulations: S1 is fed by upright line convection, L1, from the boundary layer; S2a and S2b occasionally triggered further elements of line convection, L2 (not shown); S3 is fed by shallow convection in the cold air. The jagged line at low levels between 1130 and 1330 UTC highlights the upper boundary of low-level convection. All of the slantwise circulations occur within an intense cold-frontal zone which is connected to a pronounced tropopause fold. The tropopause is highlighted by a solid line, broken at 1240 UTC where it folds. The region above the tropopause is seen to be characterized by a highly laminated structure in radar echo power because of the high static stability there. The cloud turrets sketched at upper levels between S1 and the tropopause correspond to upright convective cells associated with the satellite-detected cloud-top striations which tend to be in bands aligned roughly parallel to the plane of the diagram.

useful context for the Aberporth sounding is provided by the time–height section for nearby Aberystwyth in Fig. 13. The arrows in Fig. 13 show RSA flows derived from a high-resolution version of Fig. 6(a) (these flows are superimposed on VHF radar echo power which we shall explain shortly). If the sounding in Fig. 12 is compared with the RSA flows at 1100 UTC in Fig. 13, a close correspondence can be seen between the features labelled S in both figures.

The reason for plotting echo power as a background to Fig. 13 is that the echo intensity at VHF is determined by the static stability (and, in the lower troposphere, by any associated humidity gradients), and the echo pattern gives an indication of the laminar structure of the atmosphere. The interpretation of the echo pattern is not straightforward and it is difficult to make sense of all the details in Fig. 13; however, a few key points emerge. First of all, multiple echo layers show up in the lower stratosphere and the lowest of these corresponds to the tropopause (Vaughan *et al.* 1995), which is highlighted in Fig. 13 by solid curves. Other stable layers also show up in the troposphere, notably the sloping layers parallel to, and below, the S3 flow. According to Fig. 12, the boundaries of flows S1 and S2a were also characterized by shallow stable layers, but Fig. 13 suggests that any associated echo layers were being distorted by irregularities in the RSA flows, perhaps because they were composed of the aggregated outflow from multiple elements of line convection. The intense echoes

below 4 km, from 1100 to 1315 UTC, are probably from the edges of boundary-layer convection, some of which may have fed the flow S3. The intense echo between 4 and 6 km, around 1200 UTC, appears to be located where the S2a moist flow encountered the dry subsiding air in the tropopause fold. Finally, the region of upper-level convection, diagnosed previously as occurring between the S1 flow and the tropopause, is seen to be associated with low echo power, presumably because this is a region of low static stability.

4. Concluding synthesis

In this study we have identified a number of convective structures organized on the mesoscale as listed below. The inter-relationship of these features is summarized in Fig. 13, where the labelling corresponds to that used in section 3 and the various features are superimposed on a background of received-power for the VHF radar at Aberystwyth.

The main features are as follows:

(1) *Primary slantwise convection (S1)*: a persistent layer of rearward-sloping ascent (RSA) producing a wide cold-frontal rainband and feeding into the main upper-level jet. A shallow layer of forward-sloping descent (not labelled) underlies S1.

(2) *Primary line convection (L1)*: a persistent line of upright convection producing a narrow cold-frontal rainband consisting of a chain of elongated cores of heavy rain, and associated with strong boundary-layer convergence and cyclonic shear at the edge of a low-level jet with high θ_w. The depth of the upright convection varies between 3 and 5 km; at times, it may be absent altogether, but when it exists it feeds the slantwise convection, S1.

(3) *Secondary slantwise convection (S2)*: a persistent layer (or layers) of rearward-sloping ascent (with forward-sloping descent beneath) situated about 2 km below the primary (and stronger) slantwise circulation. (A further circulation, S3, occurred behind S2.)

(4) *Secondary line convection (L2)*: an intermittent and much weaker version of L1 (not shown in Fig. 13) which occasionally feeds into (and perhaps is triggered by) S2. The narrow cold-frontal rainband due to L2, when it occurs, is embedded within the main wide cold-frontal rainband.

(5) *Upper-level convective cells*: these occur at the top of the primary slantwise convection (and sometimes also above the secondary slantwise convection). In the intense cold-frontal cases studied in this paper, the upper-level convective cells are organized into bands 30 to 55 km apart, giving rise to satellite-detected *cloud-top striations* orientated roughly parallel to the wind shear at cloud-top level (in the layer 9 to 9.5 km in Fig. 10), and situated immediately below the tropopause.

Features S1 and L1 are well-known and summarized in reviews (e.g. Browning 1990). Features S2 and L2 are less well known but evidence is accumulating that the multilayered structures with multiple (generally weak) lines of boundary-layer convection are common in cold-frontal zones (e.g. Browning *et al.* 1995, 1998, 2001a, 2001b). According to Browning *et al.* (2001a), circulation S1 occurs within a broad zone of frontogenetically forced ascent, locally enhanced by the release of CSI (Bennetts and Hoskins 1979) and by a process of ΔM adjustment whereby air lofted by L1 is subgeostrophic at the top of the line convection and ascends slantwise in order to restore geostrophic balance (Holt and Thorpe 1991). The greater intermittency of the secondary line convection, L2, suggests that this line convection is generally not the main cause of S2; rather S2 is more likely to be due to the release of CSI. The mesoscale circulations

corresponding to S1 and S2 presumably generate regions of potential instability by distorting the θ_w surfaces as suggested by Bennetts and Hoskins (1979). The release of this instability manifests itself as upper-level convective cells which, as shown in the present study, may become organized into striations roughly parallel to the local shear just beneath the tropopause at cloud-top level but normal to the thermal-wind shear in the underlying frontal zone. It is not known what determines the large wavelength of the striations.

Cloud-top striations resembling those studied here were first identified by Feren (1995) and they correspond to those analysed more recently by Dixon *et al.* (2000). Their importance lies in the fact that they may constitute a signature of vigorous mesoscale circulations likely to be associated with situations of adverse weather.

ACKNOWLEDGEMENT

C.-G. Wang was funded by Natural Environment Research Council through its support of the Universities Weather Research Network (UWERN).

REFERENCES

Bader, M. J., Forbes, G. S., Grant, J. R., Lilley, R. B. E. and Waters, A. J. 1995 *Images in weather forecasting*. Cambridge University Press, Cambridge, UK

Bennetts, D. A. and Hoskins, B. J. 1979 Conditional symmetric instability—a possible explanation for frontal rainbands. *Q. J. R. Meteorol. Soc.*, **105,** 945–962

Browning, K. A. 1990 Organisation of clouds and precipitation in extratropical cyclones. Pp. 129–153 in *Extratropical cyclones*. Eds. C. W. Newton and E. O. Holopainen. American Meteorological Society, Boston, USA

Browning, K. A. and Harrold, T. W. 1970 Air motion and precipitation growth at a cold front. *Q. J. R. Meteorol. Soc.*, **99,** 369–389

Browning, K. A. and Pardoe, C. W. 1973 Structure of low-level jet streams ahead of mid-latitude cold fronts. *Q. J. R. Meteorol. Soc.*, **99,** 619–638

Browning, K. A., Clough, S. A., Davitt, C. S. A., Roberts, N. M., Hewson, T. D. and Healey, P. G. W. 1995 Observations of the mesoscale sub-structure in the cold air of a developing frontal cyclone. *Q. J. R. Meteorol. Soc.*, **121,** 1229–1254

Browning, K. A., Jerrett, D., Nash, J., Oakley, T. and Roberts, N. M. 1998 Cold frontal structure derived from radar wind profilers. *Meteorol. Appl.*, **5,** 67–74

Browning, K. A., Chapman, D. and Dixon, R. S. 2001a Stacked slantwise convective circulations. *Q. J. R. Meteorol. Soc.*, **127,** 2513–2536

Browning, K. A., Dixon, R. S., Gaffard, C. and Wang, C.-G. 2001b Wind profiler measurements in the storm of 30 October 2000. *Weather*, **56,** 367–373

Dixon, R. S., Browning, K. A. and Shutts, G. J. 2000 The mystery of striated cloud heads in satellite imagery. *Atmos. Sci. Lett.*, **1,** Electronic Journal

Feren, G. 1995 The striated-delta cloud system—a satellite imagery precursor to major cyclogenesis in the Eastern Australian–Western Tasmanian Sea region. *Weather Forecasting*, **10,** 286–309

Goddard, J. W. F., Eastment, J. D. and Thurai, M. 1994 The Chilbolton advanced meteorological radar: a tool for multi-disciplinary research. *Electron. & Commun. Eng. J.*, **6,** 77–86

Hobbs, P. V. 1978 Organisation and structure of clouds and precipitation on the mesoscale and microscale in cyclonic storms. *Rev. Geophys. and Space Phys.*, **16,** 741–755

Holt, M. W. and Thorpe, A. J. 1991 Localized forcing of slantwise motion at fronts. *Q. J. R. Meteorol. Soc.*, **117,** 943–963

Koch, S. E. and O'Handley, C. 1997 Operational forecasting and detection of mesoscale gravity waves. *Weather and Forecasting*, **12,** 253–281

Miles, J. W. and Howard, L. N. 1964 Note on a heterogeneous shear flow. *J. Fluid. Mech.*, **20,** 331–336

Shapiro, M. A. and Keyser, D. 1990 Fronts, jet streams and the tropopause. Pp. 167–191 in *Extra-tropical cyclones*. Eds. C. W. Newton and E. O. Holopainen. American Meteorological Society, Boston, USA

Slater, K., Stevens, A. D., Pearmain, S. A. M., Eccles, D., Hall, A. J., Bennett, R. G. T., France, L., Roberts, G., Olewicz, Z. K. and Thomas, L. 1991 'Overview of the MST radar system at Aberystwyth'. Pp. 479–482 in Proceedings of the fifth workshop on technical and scientific aspects of MST radar. Ed. B. Edwards. SCOSTEP, University of Illinois, Urbana, USA

Vaughan, G., Howells, A. and Price, J. D. 1995 Use of MST radars to probe the mesoscale structure of the tropopause. *Tellus*, **47A,** 759–765

Wakimoto, R. M. and Bosart, B. L. 2000 Airborne radar observations of a cold front during FASTEX. *Mon. Weather Rev.*, **128,** 2447–2470

Wallace, J. M. and Hobbs, P. V. 1977 *Atmospheric science: An introductory survey*. Academic Press, New York, USA